Simulating impacts of wind farms on local hydrometeorology

Somnath Baidya Roy*

Department of Atmospheric Sciences, University of Illinois, 209 S. Gregory St., Urbana, IL 61801, USA

ARTICLE INFO

ABSTRACT

Wind power is one of the fastest growing energy sources in the world, most of the growth being in large wind farms that are often located on agricultural land near residential communities. This study explores the possible impacts of such wind farms on local hydrometeorology using a mesoscale model equipped with a rotor parameterization based on data from a commercial wind turbine. Results show that wind farms significantly affect near-surface air temperature and humidity as well as surface sensible and latent heat fluxes. The signs of the impacts, i.e., increase or decrease, depend on the static stability and total water mixing ratio lapse rates of the atmosphere. The magnitudes of these impacts are not only constrained by the hub-height wind speed but also depend to some extent on the size of the wind farms. Wind farms also affect the hydrometeorology of an area up to 18–23 km downwind. More work is required to conclusively estimate the length-scale of wind farm wakes. This study is one of the first few to provide realistic estimates of possible impacts of wind farms. The model developed and used in this study can help in assessing and addressing the environmental impacts of wind farms thereby ensuring the long-term sustainability of wind power.

© 2010 Elsevier Ltd. All rights reserved.

1. Introduction

Studies with global and regional climate models have shown that extremely large wind farms may have strong impacts on weather and climate at local, regional and global scales (Baidya Roy et al., 2004; Keith et al., 2004; Adams and Keith, 2007; Kirk-Davidoff and Keith, 2008; Barrie and Kirk-Davidoff, 2010; Wang and Prinn, 2010). A recent study by Baidya Roy and Traiteur (2010) was the first to provide observational evidence of meteorological impacts of wind farms. The observations were taken at 2 towers, one upwind and another downwind of the wind farm. Additionally, that study showed that the impacts are caused by enhanced vertical mixing due to turbulence in the wake of wind turbine rotors.

Existing studies have used 2 different approaches to incorporate wind farms in atmospheric models. In both of these approaches wind farms are parameterized as subgrid-scale features. This is unavoidable because the horizontal spatial resolution of atmospheric models is too coarse to resolve wind turbines and wind farms. Studies with global climate models (Keith et al., 2004; Adams and Keith, 2007; Kirk-Davidoff and Keith, 2008; Barrie and Kirk-Davidoff, 2010; Wang and Prinn, 2010) have used a roughness-length approach where wind farms are represented by grid cells with high roughness lengths. The major challenge in

this approach is to find values of roughness length appropriate for wind farms. In contrast, Baidya Roy et al. (2004) and Baidya Roy and Traiteur (2010) have parameterized individual rotors as elevated sinks of momentum and sources of turbulent kinetic energy (TKE). Their rotor parameterization is intuitive but very idealized because it assumes a constant coefficient of performance (C_p) that is likely to produce unrealistic estimates of the impacts of wind farms.

The current study improves upon the Baidya Roy and Traiteur (2010) study by using a realistic rotor parameterization based on data from a late-model commercial turbine. Using a regional climate model equipped with a state-of-the-art microphysics and land-surface scheme this study also looks at the impacts of wind farms on near-surface temperature, humidity and surface fluxes of sensible and latent heat. This effort is in contrast with Baidya Roy and Traiteur (2010) that exclusively focused on air temperature. Additionally this study also examines the spatial distribution of the impacts within and downwind of the wind farms especially focusing on the importance of the spatial scale of wind farms.

Wind and other renewable energy sources are likely to be a part of the solution of the atmospheric carbon and climate change problem (Pacala and Socolow, 2004). Hence, wind power features prominently in the future energy plans of all industrial economies (Global Wind, 2008). It is currently one of the fastest growing energy sources in the world and will continue to do so in the near future. Most of the growth is in the utility sector (Wiser et al., 2007) consisting of large turbines and farms that are continuously increasing in power generation capability and spatial scale.

* Tel.: +1 2172441123.
E-mail address: sbroy@atmos.uiuc.edu

This study will improve our understanding of how these mega-structures interact with atmospheric boundary layer (ABL) dynamics and thermodynamics and provide realistic quantitative estimates of the possible impacts of wind farms on local hydrometeorology. The findings of this study will play a critical role in developing strategies to address these impacts thereby ensuring the long-term sustainability of wind power.

2. Impacts of wind farms on surface hydrometeorology

2.1. Model description and configuration

The Regional Atmospheric Modeling System or RAMS (Cotton et al., 2003; Pielke et al., 1992) was used to conduct a set of 306 simulations to investigate the impact of wind farms on local hydrometeorology. RAMS solves the full three-dimensional, compressible, nonhydrostatic dynamic equations, a thermodynamic equation and a set of microphysics equations. The system was closed with the Mellor-Yamada level 2.5 scheme (Mellor and Yamada, 1977) that explicitly solves for TKE while parameterizing other second-order moments. The coordinate system was rectangular Cartesian in the horizontal and terrain-following σ-type (Clark, 1977) in the vertical. The lateral atmospheric boundary conditions were zero-gradient inflow-outflow type following Klemp and Wilhelmson (1978). The bottom boundary conditions were supplied by LEAF3, the Land Ecosystem–Atmosphere Feedback model (Walko et al., 2000) version 3, dynamically coupled with RAMS. Radiative transfer within the atmosphere was simulated with a 2-stream scheme (Harrington, 1997) that treats the interaction of 3 solar and 5 infrared bands with atmospheric gases and hydrometeors. A detailed bulk microphysics scheme (Walko et al., 1995; Meyers et al., 1997) was used to prognose mixing ratio and number concentration of 7 different species of moisture and interactions between them in the atmosphere.

RAMS was used to simulate a rectangular domain, 107 km in the zonal (west–east) direction and 23 km in the meridional (south–north) direction, discretized in the horizontal with 1 km spacing (Fig. 1). The zonal alignment of the rectangular domain as well as the wind farm provides distinct computational advantages that are discussed later in this section. The vertical grid consisted of 19 layers of varying thickness. The heights of the atmospheric levels are shown in Table 1. With 9 layers in the lowest 1 km, this vertical grid can adequately resolve small-scale turbulent processes in the ABL. For simplicity, the domain was assumed to be a flat terrain at sea-level covered with bare soil.

The simulated wind farm was designed to be approximate a 7×3 array of the Gamesa G80-2.0 MW wind turbines (Gamesa 2010) spaced 1 km apart. According to the specifications, each G80-2.0 MW turbine is 100 m tall with 40 m rotor blades (80 m rotor diameter).

The 1-km spacing (12.5 rotor diameter) used in this study is slightly larger but not unrealistic compared to current recommended standards (Denholm et al., 2009). The wind farm was represented by introducing a rotor parameterization in the third atmospheric layer of a 7×3 array of grid cells in the center of the domain. The rotors were represented by a subgrid parameterization that assumes a rotor to be an elevated sink of momentum and a source of TKE. The rotor parameterization was implemented as follows:

- The turbines occupied 21 grid cells in the center of the model domain with a rotor located in the third atmospheric layer of each grid column. This layer is 80 m thick and located at a height of 100 m. Thus, the rotors can be completely contained within these grid cells.
- At each model timestep, the volume of air passing through the rotor is $\Delta V = \pi R^2 |\overrightarrow{U}| \Delta t$, where R=length of rotor blade, $\overrightarrow{U}$=wind velocity in the third atmospheric layer (wind turbine hub-height), and Δt=model timestep.
- The mass of the said volume of air is $\Delta M = \rho \Delta V$ where ρ is the density of air.
- The resolved kinetic energy (RKE) of the air passing through the rotor: $\Delta E = 1/2 \Delta M |\overrightarrow{U}|^2$.
- If $4 \, \text{m s}^{-1} < |\overrightarrow{U}| < 25 \, \text{m s}^{-1}$, then δE energy is removed from the atmospheric flow for generating power. The value of δE is calculated by simple linear interpolation from the power curve data of the Gamesa G80–2.0 MW turbine (Gamesa, 2010).

Table 1
Heights of the RAMS model atmospheric levels.

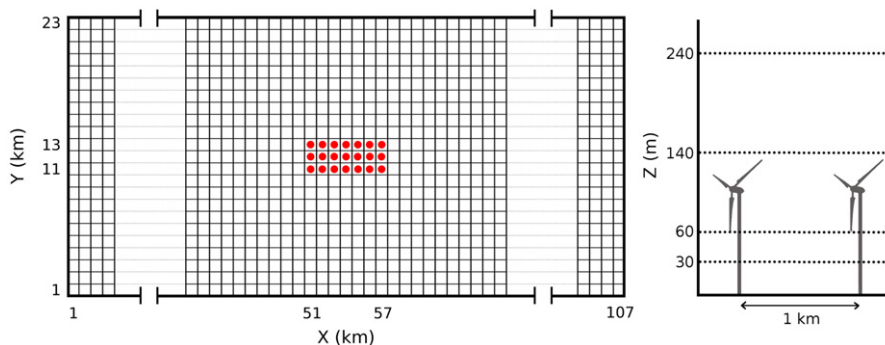| Model level	Height (m)
1	0
2	30
3	60
4	140
5	240
6	350
7	470
8	614
9	786
10	994
11	1242
12	1541
13	1899
14	2329
15	2845
16	3465
17	4208
18	5099
19	6169

Fig. 1. Schematic diagram of (left) horizontal grid structure with the grid cells containing the rotors marked by the red circles in the middle and (right) vertical grid structure showing the lowest 4 atmospheric layers.
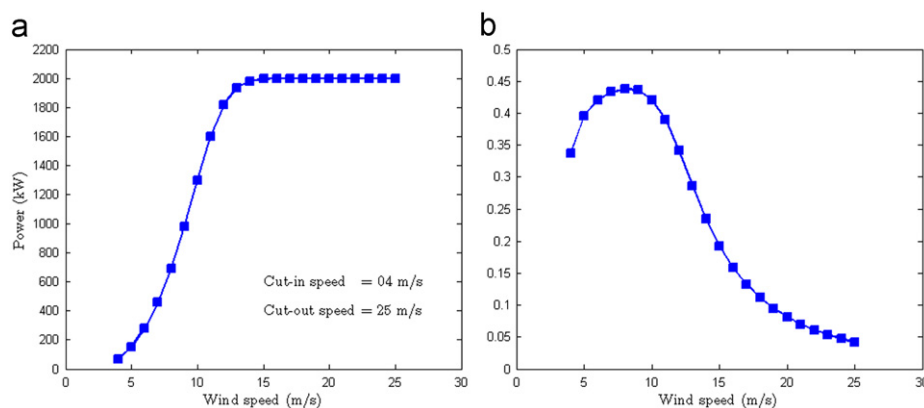
Fig. 2. (a) Power curve and (b) coefficient of performance of the Gamesa G80-2.0 MW turbine as a function of hub-height wind speed. Calculations were made assuming air density = 1.225 kg/m^3.

The fraction of energy passing through the rotor that is captured for power generation by turbines is known as the coefficient of performance (C_p). C_p is a function of wind speed and rotor design, reaching a maximum of 16/27, known as the Betz Limit (Frandsen, 1992). Fig. 2 shows that the C_p of the Gamesa G80-2.0 MW turbine reaches a maximum of about 0.45 at 10 m/s wind speeds but falls rapidly to less than 0.05 at high wind speeds. It is important to note that the power curve of a wind turbine refers to electrical power. The aerodynamic power absorbed by the turbine is larger by about 10% accounting for gearbox and generator losses (Hau, 2005).

- Observations from the San Gorgonio wind farm show that the TKE of the air passing through the rotor is approximately 5 m^2 s^{-2} higher than the ambient value and remains fairly constant with varying wind speeds (Baidya Roy et al., 2004). Similar values have been reported by Taylor (1983). Thus, TKE generated in the entire wake due to turning of the rotor can be represented by $\Delta e = 5\rho\Delta V$.
- The TKE of the grid cell can now be calculated as $e_1 = e_0 + \Delta e/\rho V$, where e_0 and e_1 are the TKEs of the grid cell before and after the rotor parameterization subroutine is called, respectively, and V is the volume of the grid cell.
- The RKE of the grid cell containing the rotor decreases because δE part of it is removed to generate electricity while Δe part is converted to turbulence in the wake. So, at the end of the timestep, the RKE of the grid cell becomes $E_1 = E_0 - \delta E - \Delta e/\rho V$, where E_0 and E_1 are the RKEs of the grid cell before and after the rotor parameterization subroutine is called, respectively.
- The wind velocity of the cell can now be calculated as $\vec{U} = \sqrt{2E_1/\rho V}$.

In the Mellor-Yamada (1977) closure scheme, TKE and momentum are prognosed. The rotor parameterization effectively adds a source term to the TKE equation and a sink term to the momentum equation. . The magnitude of the source/sink terms is calculated at every timestep with respect to the volume of air passing through the rotor (ΔV) but the source/sink terms are applied to the entire grid cell volume (V). It is important to note that ΔV is many orders of magnitude smaller than V. For example at a wind speed of 10 m/s, $\Delta V = 100{,}528$ m^2 but $V = 80{,}000{,}000$ m^2 and hence, ΔV is only 0.125% of V. So, when the source/sink terms are averaged over the entire grid cell at a particular timestep, they do not produce an instantaneous shock large enough to destabilize the system. However, the cumulative impact of the source/sink terms can be large if the wind speeds are sustained within the operating range of the wind turbine. The momentum deficit and TKE enhancement in the wake grows with time and alters the

Table 2
Sounding data from the following WMO stations were used to initialize the RAMS model simulations.

Station	Latitude, Longitude
Albuquerque, NM	35/02N, 106/37W
Boise, ID	43/34N, 116/13W
Denver Int. Airport, CO	39/46N, 104/52W
Desert Rock, NV	36/37N, 116/01W
Elko, NV	40/52N, 115/44W
Flagstaff, AZ	35/14N, 111/49W
Glasgow, MT	48/13N, 106/37W
Grand Junction, CO	39/07N, 108/32W
Great Falls, MT	47/27N, 111/23W
Medford, OR	42/23N, 122/53W
Oakland, CA	37/45N, 122/13W
Quillayute, WA	47/47N, 124/33W
Reno, NV	39/34N, 119/48W
Riverton, WY	43/04N, 108/29W
Salem, OR	44/55N, 123/01W
Salt Lake City, UT	40/47N, 111/57W
San Diego, CA	32/50N, 117/07W
Santa Teresa, NM	31/52N, 106/42W
Spokane, WA	47/38N, 117/32W
Tucson, AZ	32/07N, 110/56W
Vandenberg AFB, CA	34/44N, 120/33W

mean momentum and TKE of the entire grid cell, thereby significantly affecting the vertical transport of heat and moisture.

The simulations were initialized with atmospheric sounding data for November 1, 2008, February 1, May 1 and August 1, 2009, from 21 World Meteorological Organization (WMO) stations in western US (Table 2). These observations are taken by radiosondes that are small automated disposable sensors attached to weather balloons. These sensors sample the air every 5 s while the balloon is ascending and transmit the data to ground-based data acquisition and processing centers. Depending on the speed of ascent, the vertical spatial resolution of the data is in the 10–100 m range in the troposphere. The sensors record a wide array of atmospheric dynamic and thermodynamic properties of which pressure, temperature, relative humidity, wind speed and wind direction were used for model initialization. Only the wind directions in the input soundings were changed to 270° so that all wind was assumed to be westerly, i.e. blowing from west to east. This assumption, in conjunction with the zonal (west–east) orientation of the model domain and the simulated wind farm optimizes computational costs against experimental requirements. In this configuration, the wind farm is 50 km away from both the inflow (western) and outflow (eastern) boundaries. Thus perturbations from the inflow boundary are less likely to affect the wind farm and the wind farm wake is less likely to affect the

outflow boundary. The meridional (south–north) transport of perturbations is mainly by diffusion due to the absence of meridional wind. This is a slow process and hence the wind farm can be placed closer to the domain boundaries. This allows for a rectangular 107 km × 23 km computational domain, as opposed to a square 107 km × 107 km domain thereby saving a considerable amount of computing resources.

The input soundings were available for 0Z and 12Z, corresponding to 4 or 5 am (0Z) and 4 or 5 pm (12Z) local standard time, depending on whether the stations were in the US Mountain or Western Standard time zones. In total, 153 complete soundings were available covering the entire annual cycle. The model was integrated for 1 h with a timestep of 2 s. For each initial condition, a pair of simulations was conducted: one with the rotor parameterization switched off (control) and another with the parameterization turned on (wind farm case).

2.2. Results

A comparison of each pair of wind farm and control simulations was conducted to study the effect of wind farms on near-surface temperature, humidity and surface sensible and latent heat fluxes as a function of ambient atmospheric flow parameters. In the context of the RAMS model simulations, near-surface refers to the lowest model level centered at a height of 15 m above the ground surface. For each simulation, the 4 variables were averaged in space over the 21 points corresponding to the wind farm location as well as in time over the entire simulation period. The impact of wind farms was then quantified by calculating the differences in these 4 space-time averaged variables between *each pair* of control and wind farm simulations. Ambient lapse rate and hub-height wind speed were calculated from each

control simulation by averaging over the 21 points corresponding to the location of the wind farms. Only the lapse rate in the lowest 350 m layer was considered because this layer is likely to be the most affected due to the turbulent rotor wakes. The 0–350 m lapse rate was calculated as the equivalent potential temperature (θ_e) gradient between the 1st and the 5th atmospheric levels.

Baidya Roy et al. (2004) and Baidya Roy and Traiteur (2010) found that the impacts at the surface are due to the enhanced vertical mixing generated by the turbulence in the wakes of the spinning rotors. Consider a statically stable environment where temperature increases with height. Turbulence will mix warm air down and cool air up leading to a warming at the surface and a cooling aloft. The opposite will occur when the atmosphere is statically unstable. This phenomenon is clearly evident in Fig. 3a where we see a general increase in surface temperatures under positive lapse rates and a decrease under negative lapse rates. This result is qualitatively similar to Baidya Roy and Traiteur (2010) but a quantitative comparison is not appropriate because the simulations in the present study are significantly different due to inclusion of moisture effects. In this figure, θ_e is used instead of actual temperature as a measure of environmental stability. Equivalent potential temperature of an air parcel is defined as the temperature a parcel of air would have if it is transported adiabatically from its current altitude at pressure p to the standard pressure level p_0 and all the water vapor in the parcel condenses, releasing its latent heat. Mathematically, θ_e is given by

$$\theta_e \approx \left(T + \frac{L_v}{C_p}r\right)\left(\frac{p_0}{p}\right)^{R_d/C_p}$$

where T is the temperature of the parcel at pressure p, r is the mixing ratio, p_0 is the standard reference pressure equal to 100 kPa, L_v is the latent heat of vaporization, C_p is the specific
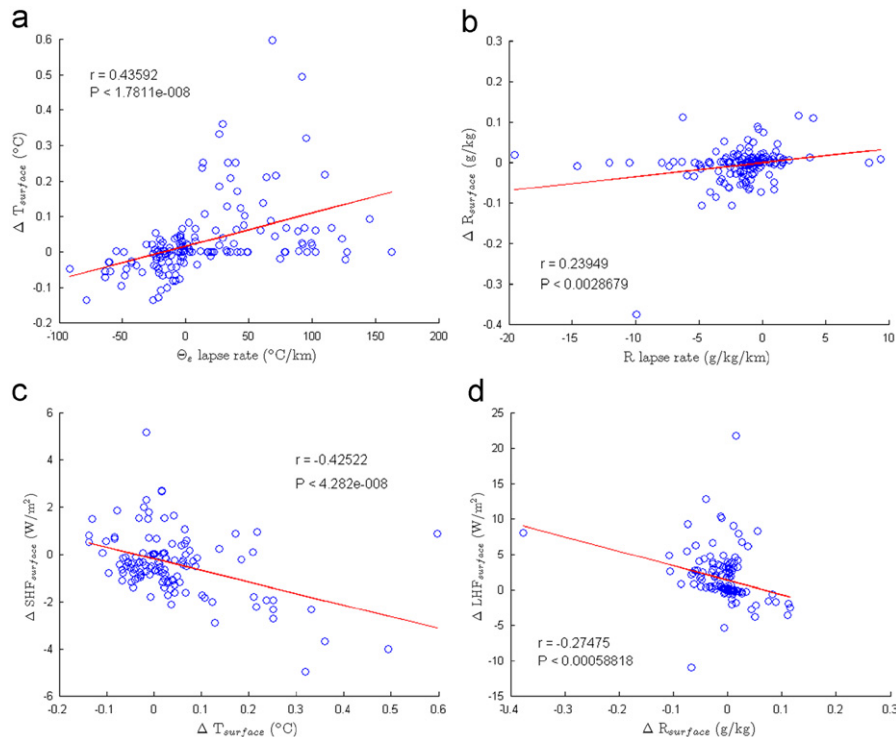
Fig. 3. Scatter plot showing the relationship between (a) the change in near-surface air temperature and the ambient 0–350 m equivalent potential temperature lapse rate; (b) the change in near surface total water mixing ratio and the ambient 0–350 m total water mixing ratio lapse rate; (c) the change in surface sensible heat flux and the change in near-surface air temperature; and (d) the change in surface latent heat flux and the change in near surface total water mixing ratio. The scatter plots consist of 153 points, each of which represents the difference between the control and wind farm simulation for a particular initial condition. These differences are averaged over the 21 points corresponding to the location of the wind farm and the 1-h simulation period. Statistical significance of the correlation coefficient was estimated using the Student's *t*-test.

heat of dry air at constant pressure and R_d is the specific gas constant for air. θ_e is conserved during moist adiabatic transport. Since almost all atmospheric transport is moist adiabatic, θ_e lapse rate is the most appropriate measure of atmospheric stability (Wallace and Hobbs, 2006). Thus, the change in surface air temperature (ΔT) exhibits a statistically significant positive correlation with θ_e lapse rate.

The same phenomenon can be observed in Fig. 3b showing the relationship between change in surface total water mixing ratio (R) and the ambient mixing ratio lapse rate. Total water mixing ratio, defined as the amount of moisture present in each kg of dry air, is a measure of water content of an air parcel. If the R lapse rate is positive, i.e., humidity increases with height, turbulence mixes relatively moist air down and relatively dry air up, leading to a net moistening of near-surface air and vice versa. Thus, the change in surface humidity (ΔR) shows a statistically significant positive correlation with respect to R lapse rate.

Change in near-surface air temperature and humidity has a strong impact on the fluxes of sensible and latent heat between the ground and the atmosphere. Surface sensible heat flux (SHF) is a function of the gradient between the ground and the near-surface air temperatures. Consider a typical late afternoon (4 pm) scenario when the temperature has a negative lapse rate and the ground is warmer than the air above it. Hence, the surface sensible heat flux is positive, i.e., heat is transported from the ground to the atmosphere. Under this condition, wind farms produce a cooling effect on the near-surface air temperatures, thereby increasing the ground-air temperature gradient. Consequently, more heat is transported from the ground to the atmosphere, i.e., the surface sensible heat flux increases. On the other hand, during early mornings (4 am), the lapse rate is typically positive and the surface sensible heat flux is negative because the air is warmer than the ground. As described earlier, wind farms lead to a warming of the surface air, making both the ground-air temperature gradient and the surface sensible heat flux more negative. Thus a positive ΔT near the surface leads to a negative ΔSHF and vice versa. This phenomenon is demonstrated in Fig. 3c where ΔT and ΔSHF exhibit a statistically significant negative correlation. By similar logic, near-surface ΔR and surface latent heat flux (LHF) are negatively correlated as well (Fig. 3d). LHF is driven by ground-air moisture gradient. Thus, LHF increases due to a drying of the near-surface air and decreases due to an increase in near-surface R values.
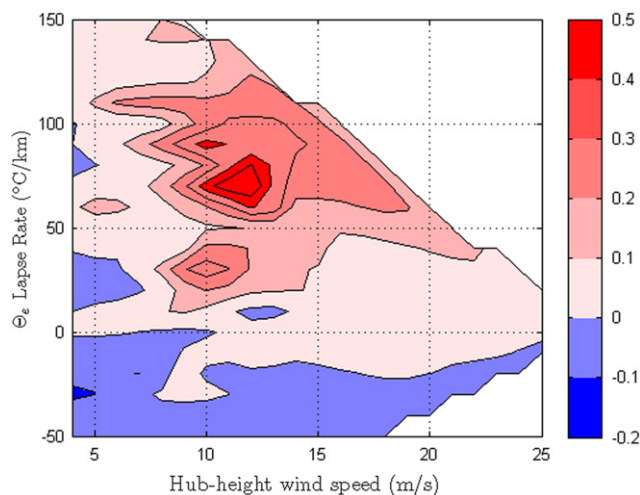

Fig. 4. Change in near-surface air temperature (°C) averaged over the entire wind farm plotted as a function of ambient 0–350 m equivalent potential temperature lapse rate (°C/km) and turbine hub-height wind speed (m/s).

Fig. 4 shows that ΔT is a function of both θ_e lapse rate and the turbine hub-height (100 m) wind speed. Maximum impacts occur at intermediate wind speeds (10–13 m/s) and intermediate positive lapse rates (~ 70 °C/km). The values of ΔT are small at very high as well as very low wind speeds. Typically high wind speeds are associated with neutral stability where θ_e lapse rate is very small. Under this condition, the atmosphere is already well-mixed and hence extra mixing by wake turbulence has little to no impact on near-surface air temperatures. At very weak wind speeds, even though the lapse rates can be very high, the impacts are small. This is because the rotors probably function intermittently as the wind speeds frequently drop below the cut-in speed of the Gamesa G80-2.0 MW turbine.

3. Effect of wind farm size

The previous analysis deals with the mean hydrometeorological impacts within a small wind farm. A series of sensitivity studies were conducted to explore 2 additional questions:

i. Does the magnitude of the impacts depend on the spatial scale of the wind farms?
ii. What is the spatial distribution of these effects within and downwind of wind farms?

In these simulations, the same model configuration as before was used. The model domain was extended to 125 km to accommodate downwind wind farm wakes. Apart from a control case, a total of 5 other simulations were conducted with wind farms of length $\lambda = 5$, 10, 15, 20 and 25 km where the wind farms started from the 51st grid point of the domain and extended up to the 55th, 60th, 65th, 70th and 75th grid points in the zonal (west–east) directions, respectively. They all spanned 3 grid points in the meridional (south–north) direction.

The simulations were initialized with sounding data collected on 12Z (5 am LST) August 1, 2009, from the Glasgow, Montana, NWS station. This particular dataset was used because in the previous simulation, this sounding produced the strongest impact on near-surface air temperature. The same experiments were repeated with data collected on 12Z (4 am LST) November 1, 2008 from the NWS station in Quillayute, Washington. Both cases had similar stability with positive θ_e lapse rates of similar magnitude. However, the mean hub-height wind speed at the Glasgow station (11.4 m/s) was almost double that of the Quillayute station (6.1 m/s). Additionally, the mixing ratio lapse rate was positive at Glasgow but negative at Quillayute. The results of this sensitivity study are plotted in Fig. 5 (Glasgow) and 6 (Quillayute) and match quite well with the results of the experiments discussed in the previous section. All simulations at the Glasgow station produced increased surface temperature and humidity and reduced surface sensible and latent heat flux. The Quillayute station produced a warming and drying leading to lower sensible heat flux but higher latent heat flux (Fig. 6).

The figures show that the magnitude of the impacts depends on the scale of the wind farm. In the Glasgow case, the peak magnitude increases as λ increases from 5 to 15 km but subsequently remains constant at the 15 km level for longer wind farms. For wind farms with $\lambda \leq 15$ km, the impacts increase with downwind distance from the western edge of the farms till reaching the peak at the end of the wind farms and start decreasing thereafter. For larger wind farms, the peak occurs 15 km into the wind farms, stays more or less constant at that level till the end is reached and then starts to decrease. In the Quillayute case, the peak magnitude is reached inside the 10 km wind farm. The peak impact remains approximately at that level
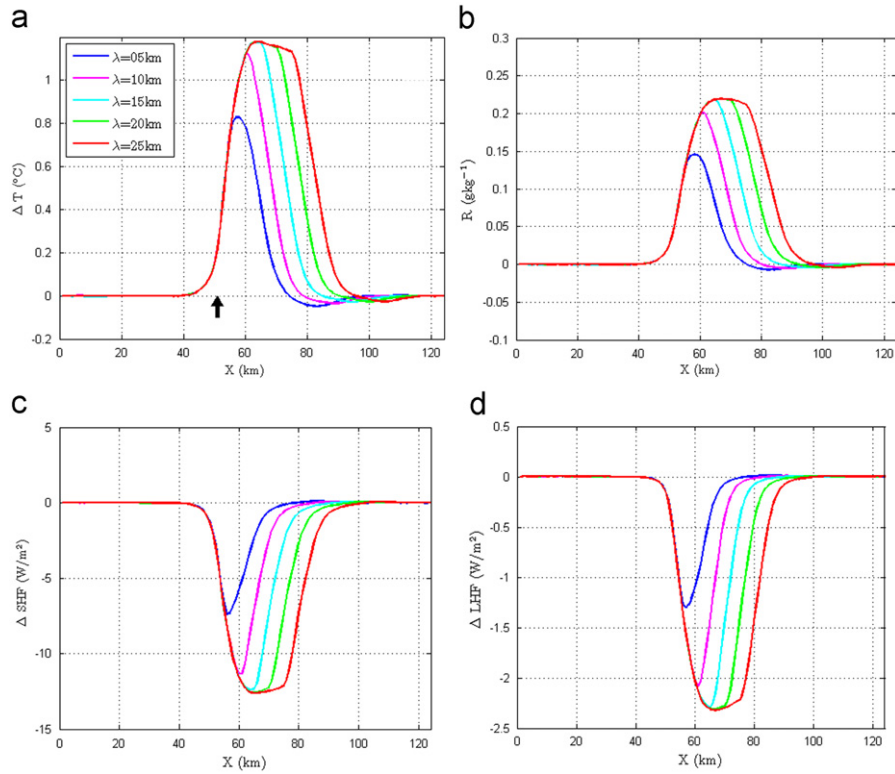
Fig. 5. Meridionally averaged changes in (a) near-surface air temperature, (b) near-surface total water mixing ratio, (c) surface sensible heat flux and (d) surface latent heat flux over wind farms of different sizes using initial conditions from 12Z August 1, 2009, from Glasgow, MT. The black arrow marks the western edge of the wind farms.
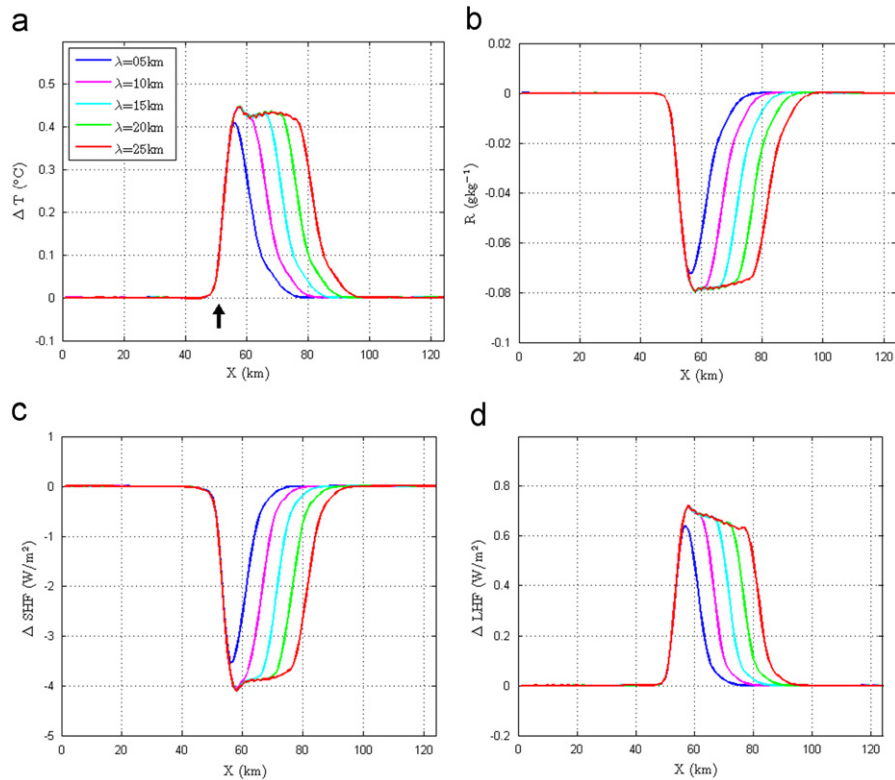

Fig. 6. Same as in Fig. 5 but with initial condition from Quillayute, WA, on 12Z November 1, 2008.

and location for larger wind farms. This pattern implies that the magnitude and location of the peak impacts is constrained by the kinetic energy of the flow, i.e., the turbine hub-height wind speed.

For small wind farms, the peak and its downwind location increase with wind farm size. Once the constraint set by the flow is reached, the peak and its location do not change however large

the wind farm may be. This pattern is evident for all 4 hydro-meteorological parameters in both locations.

While the strongest impacts occur within the wind farms, they can also be felt up to a significant distance beyond the confines of the wind farms, especially in the downwind direction. For wind farms of all size, the impacts start to decrease right at the eastern edge gradually becoming zero at a distance of 18–23 km from the edge. It appears from these simulations that the length-scale of wind farm wakes is approximately 20 km irrespective of the length-scale of the wind farms and background meteorological conditions.

4. Discussions

One of the major strengths of this work is the integration of real-world data in the rotor parameterization as well as the initial conditions to ensure that the experimental results are realistic. A typical numerical sensitivity study would have involved experimenting with different initial conditions such as keeping the lapse rate constant and linearly varying the wind speeds or using a range of lapse rates for a constant wind speed. Such studies can provide useful insights into how background meteorology affects the interactions between wind farms and atmospheric flow. However, many of these idealized experiments are likely to generate unrealistic scenarios like high wind speeds in unstable environments. By using real meteorological observations, this work produced results that are likely to be realistically observed in operational wind farms.

This study uses RAMS, a well-known mesoscale atmospheric model with the capability to simulate the interactions between wind farms and the atmospheric boundary layer. A subgrid-scale rotor parameterization is developed and implemented in RAMS to conduct numerical experiments. Subgrid parameterizations are the only way to represent rotors in mesoscale and coarser atmospheric models because wind turbine rotors and wakes are many orders of magnitude smaller than atmospheric mesoscale flow (Brand, 2007). A major advantage of RAMS and some other mesoscale models is the availability of 1.5 order closure scheme where momentum vectors and TKE are prognosed while other second-order moments representing turbulent fluxes are parameterized. The 1.5 order closure scheme allows for the implementation of the momentum sink/TKE source parameterization for wind turbine rotors. In contrast most climate models use a 1st order closure with no prognostic equation for TKE. Hence, studies using climate models have represented wind farms as surface roughness elements (Keith et al., 2004; Kirk-Davidoff and Keith, 2008; Barrie and Kirk-Davidoff, 2010; Wang and Prinn, 2010).

A wide range of studies have developed wind turbine wake models (Vermeer et al., 2003; Brand, 2007; Calaf et al., 2010). Most of these models operate at very high spatial resolution that can resolve the wakes. Some of the computational fluid dynamics models can even resolve individual rotor blades. Some of them use a 2nd order closure capable of prognosing turbulent transport. These models can resolve the 3-dimensional spatial structure of turbine wakes. However, these models are computationally too expensive to conduct a large ensemble of simulations to study the impacts of wind turbines on atmospheric flow under a wide range of initial and boundary conditions. Most importantly, the existing wake models focus entirely on the dynamics of atmospheric flow. In order to study the impact of wind farms on local hydrometeorology a model that also represents atmospheric thermodynamics and heat and moisture fluxes within and across model boundaries is required. Hence, there is a need for developing high-resolution models capable of simulating the aerodynamic and thermodynamic properties of wind turbine wakes.

These models will have to be calibrated with data from field campaigns and wind tunnels capable of incorporating non-neutral thermal stratification. It would be interesting to see if outputs from these high-resolution models, when averaged over appropriate spatial scales, can match the results from mesoscale and climate models.

Two aspects of the rotor parameterization used here needs to be explored further. First, the turbine power curve quite likely underestimates the momentum sink term. The power curve gives the electrical power output from the turbine as a function of wind speed. The aerodynamic power loss from the atmospheric flow is larger than the electrical power generated because some of the power is lost by generators and gearboxes. Field or laboratory observations are required to accurately estimate the aerodynamic power loss as a function of wind speed. Alternatively, sensitivity studies can be conducted to estimate the uncertainties generated by inaccuracies in the momentum sink term. Second, a constant TKE source is used in this work. Observations from San Gorgonio show that increase in TKE in the wind farm wake changes little with wind speed. However, this phenomenon may be unique to the location and period of the field campaign.

Even though this work uses 153 different sounding profiles, it is not an exhaustive set by any means. Other types of meteorological situations are certainly possible. One particular phenomenon of interest to wind energy companies is the low-level jet (LLJ, Stull, 1993). It is a low-altitude band of very high speed wind overlying a stable ABL such as the Great Plains nocturnal jet in the US and the Somali Jet in East Africa. There was no evidence of jets in the sounding data. It is possible that the lengthscales of wind farm wakes may exhibit a dependence on wind speeds in the presence of very strong winds. Hence there is a need for continuing this investigation with other kinds of initial conditions.

Another issue that demands a follow-up investigation is the question of time-scale. This study considers processes with time-scales of 1 h or less. Over longer timescales the response of the land surface and consequently, the effects on near-surface air temperature and humidity may be significantly different. To study these processes, the model needs to be driven by appropriate boundary conditions reflecting large-scale weather systems passing through the simulation domain.

5. Conclusions

This study uses a regional climate model to explore the possible impacts of wind farms on local hydrometeorology. A subgrid-scale rotor parameterization based on data from a commercial wind turbine was developed and implemented in the model for this study. Numerical experiments show that wind farms generate statistically significant impacts on near-surface air temperature and humidity as well as surface sensible and latent heat fluxes. These impacts depend on the atmospheric lapse rates of equivalent potential temperature and total water mixing ratio. Sensitivity studies show that these impacts are not confined to the wind farms but extend a significant distance downwind. The typical length-scale of the wind farm wakes is approximately 20 km that is independent of the size of the wind farms as well as background meteorology. However, more simulations with a wider range of initial conditions are required to conclusively demonstrate this phenomenon.

This study has significant implications for future energy and land use policy. Data show that wind power is on the verge of an explosive growth, especially in the US with many wind farms are coming up over agricultural lands. Impacts from wind turbines on surface meteorological conditions are likely to affect agricultural practices as well as communities living in residential areas

around the farms. Current research on impacts of wind farms on weather and climate primarily looks at global-scale impacts from extremely large wind farms. This study is one of the first few to provide realistic estimates of possible impacts of wind farms. The model developed and used in this study can help in assessing and addressing the environmental impacts of wind farms thereby ensuring the long-term sustainability of wind power.

References

Adams, A.S., Keith, D.W., 2007. Wind energy and climate: modeling the atmospheric impacts of wind energy turbines. EOS Trans., 2007. AGU 88.

Baidya Roy, S., Pacala, S.W., Walko, R.L., 2004. Can large wind farms affect local meteorology? J. Geophys. Res., 109. doi:10.1029/2004JD004763.

Baidya Roy, S.B., Traiteur, J.J., 2010. Impact of wind farms on surface air temperatures. Proc. Natl. Acad. Sci.. doi:10.1073/pnas.1000493107.

Barrie, D., Kirk-Davidoff, D.B., 2010. Weather response to a large wind turbine array. Atmos. Chem. Phys. 10, 769–775.

Brand, A.J., 2007. Modeling the effect of wind farming on mesoscale flow Part1: flow model. J. Phys. Conf. Ser. 75, 012043.

Calaf, M., et al., 2010. Large-eddy simulation study of fully developed wind-turbine array boundary layers. Phys. Fluids 22 (015110), 2010. doi:10.1063/1.3291077.

Clark, T.L., 1977. A small-scale dynamic model using a terrain-following transformation. J. Comput. Phys. 24, 186–215.

Cotton, W.R., et al., 2003. RAMS 2001: current status and future directions. Meteorol. Atmos. Phys. 82, 5–29.

Denholm P., et al. 2009. Land-use requirements of modern wind power plants in the United States. Technical Report NREL/TP-6A2-45834, National Renewable Energy Laboratory, Boulder CO, 46 pp. Available online at ⟨http://www.nrel.gov/docs/fy09osti/45834.pdf⟩ accessed on 24/12/2010.

Frandsen, S., 1992. On the wind speed reduction in the center of large clusters of wind turbines. J. Wind Eng. Ind. Aerodyn. 39, 251–265.

Gamesa, 2010. Gamesa G80-2.0 MW. Available online at ⟨http://www.gamesacorp.com/files/File/G80-ingles.pdf⟩. Accessed on September 7, 2010.

Global Wind, 2008. Global Wind Energy Council, Brussels, Belgium, 2009.

Harrington, J.Y., 1997. The effects of radiative and microphysical processes on simulated warm and transition season Arctic stratus. Ph.D. thesis, Colorado State University, Fort Collins, CO.

Hau, E., 2005. Wind Turbines: Fundamentals, Technologies, Applications, Economics. Springer, Berlin 783 pp.

Keith, D.W., et al., 2004. The influence of large-scale wind power on global climate. Proc. Natl. Acad. Sci. 101, 16115–16120.

Klemp, J.B., Wilhelmson, R.B., 1978. The simulation of three-dimensional convective storm dynamics. J. Atmos. Sci. 35, 1070–1096.

Kirk-Davidoff, D.B., Keith, D.W., 2008. On the climate impact of surface roughness anomalies. J. Atmos. Sci. 65, 2215–2234.

Mellor, G.L., Yamada, T., 1977. Development of a turbulence closure model for geophysical fluid problems. Rev. Geophys. Space Phys. 20, 851–875.

Meyers, M.P., et al., 1997. New RAMS cloud microphysics parameterization, Part II: the two-moment scheme. Atmos. Res. 45, 3–39.

Pacala, S.W., Socolow, R., 2004. Stabilization wedges: solving the climate problem for the next 50 years with current technologies. Science 305, 968–972.

Pielke, R.A., et al., 1992. A comprehensive meteorological modeling system – RAMS. Meteorol. Atmos. Phys. 49, 69–91.

Stull, R.B., 1993. An Introduction to Boundary Layer Meteorology. Kluwer, Dordrecht, pp 520-526.

Taylor, G.L., 1983. Wake and performance measurements on the Lawson-Tancred 17 m horizontal-axis windmill. IEE Proc. 130, 604–612.

Vermeer, L.J., et al., 2003. Wind turbine wake aerodynamics. Prog. Aerospace Sci. 39, 467–510.

Walko, R.L., et al., 1995. New RAMS cloud microphysics parameterization, Part I: the single moment scheme. Atmos. Res. 38, 29–62.

Walko, R.L., et al., 2000. Coupled atmosphere-biophysics-hydrology model for environmental modeling. J. Appl. Meteorol. 39, 931–944.

Wallace, J.M., Hobbs, P.V., 2006. Atmospheric Science: An Introductory Survey. Academic, Burlington VT, pp 85-86.

Wang, C., Prinn, R.J., 2010. Potential climatic impacts and reliability of very large-scale wind farms. Atmos. Chem. Phys. 10 (2053–2061), 2010.

Wiser R., et al., 2007. Annual Report on US Wind Power Installation, Costs and Performance Trends: 2006, US Department of Energy, pp. 9–10.